International Journal of Pressure Vessels and Piping 86 (2009) 769–776

Contents lists available at ScienceDirect

International Journal of Pressure Vessels and Piping

journal homepage: www.elsevier.com/locate/ijpvp

Effect of the welding heat input on residual stresses in butt-welds of dissimilar pipe joints

D. Akbari*, I. Sattari-Far

Faculty of Mechanical Engineering, Amirkabir University of Technology, Tehran, Iran

ARTICLE INFO

Article history:
Received 22 May 2008
Received in revised form
13 April 2009
Accepted 13 July 2009

Keywords:
Residual stresses
Elastic–plastic analysis
Heat input
Dissimilar butt-weld
Finite element method

ABSTRACT

This study used finite element techniques to analyse the thermo-mechanical behaviour and residual stresses in dissimilar butt-welded pipes. The residual stresses at the surface of some weld specimens were measured experimentally by using the hole-drilling method. The results of the finite element analysis were compared with experimentally measured data to evaluate the accuracy of the finite element modelling. Based on this study, a modelling procedure with reasonable accuracy was developed. The developed finite element modelling was used to study the effects of welding heat input on magnitude and distribution of welding residual stresses in butt-welded pipes made of ferritic and austenitic steels. The hoop and axial residual stresses in dissimilar pipe joints of 8 mm thick for V-groove shape were studied. It is shown that the welding heat input has a significant effect on magnitude and distribution of residual stresses in the stainless steel side of the studied joints.

1. Introduction

Dissimilar metal joints between pipes of ferritic and austenitic steels are widely used in engineering structures, for instance steam generators of power plants. Failure analyses carried out on dissimilar weld joints presented, have shown that a significant number of failures have occurred in the heat affected zone (HAZ) region on the ferritic steel side of such dissimilar weld joints [1]. Residual stresses present in the weld joints are shown to be an important contributing factor of the failures.

Welding residual stresses are formed in the structure as a result of non-uniform contractions which occur as the weld metal solidifies and cools to ambient temperature [2].

Welding residual stresses in welded structures are affected by several parameters and their interactions. In particular, the structural and material factors and welding parameters impact significantly. The structural factors include the type of geometry and its thickness, the type of welded joint and weld groove shape. Among the material factors, the mechanical and physical properties of the parent and filler materials are important to be considered. Welding process parameters include among other things, type of the process employed, welding current, welding voltage and arc travelling speed [3].

Heat input is an essential factor in quality control in arc welding. It is an important character because like preheat and interpass temperature, it influences the cooling rate which affects the mechanical properties and micro structure of the weld and HAZ, and consequently affects the residual stress distribution in the object [2].

The residual stresses in dissimilar joints are complex and difficult to predict, presumably because of differences between mechanical and physical properties of the parent and filler materials involved.

There are various ways of measuring or estimating residual stresses. Direct measurements are either semi destructive (hole drilling and indenting) or nondestructive (X-ray, neutron diffraction and ultrasonic). Analytical and numerical methods are also used. Due to complexity of problem, the analytical methods are normally used for simple geometries. By advances in computer technology (soft- and hardware), it is nowadays possible to use numerical techniques, like finite element methods, to satisfactorily calculate (estimate) the residual stresses in welded structures.

Brickstad and Josefson employed two-dimensional (2-D) axisymmetric models to numerically simulate multi-pass circumferential butt-welds of stainless steel pipes up to 40 mm thick in a non-linear thermo-mechanical finite element analysis [4]. Mochizuki et al. used inherent strain analysis and thermo-elastic–plastic analysis to predict residual stresses in carbon steel pipes, and they verified their numerical models by using neutron

* Corresponding author. Tel.: +98 21 6454 3426; fax: +98 21 6641 9736.
E-mail address: davood.akbari@gmail.com (D. Akbari).

0308-0161/$ – see front matter © 2009 Elsevier Ltd. All rights reserved.
doi:10.1016/j.ijpvp.2009.07.005

diffraction measurement [5]. Mohr estimated internal surface residual stresses in girth butt-welded steel pipes [6]. Michaleris computed residual stresses for circumferential girth welds on thin and thick walled pipes for single-V type weld joints using thermo-elastic–plastic analyses [7].

Elena and Mihaela simulated the temperature field in welded plates of carbon and austenitic steels [8]. Emil studied the welding process influence on metallurgical and mechanical modifications from dissimilar metal joints [9]. Dimitrios and Anastasius compared a simplified 2-D axi-symmetric model with a detailed 3-D model in determination of residual stresses of dissimilar weld pipe joints [10]. However, there are very limited studies on effects of welding parameters on residual stresses in dissimilar welded pipe joints.

In this work, the development of welding residual stresses in a dissimilar pipe joint made of A240-TP304 stainless steel and A106-B carbon steel is studied by using 3-D finite element method (FEM). The FEM results are compared with experimental measured data using the hole-drilling method. The effects of welding heat input on distribution and magnitude of residual stresses are studied.

2. Theoretical aspects

Theoretical considerations of the thermal and mechanical aspects that used in the FEM analysis are briefly described below.

2.1. Thermal analysis

When a volume is bounded by an arbitrary surface, the balance relation of the heat flow is expressed by:

$$-\left(\frac{\partial R_x}{\partial x}+\frac{\partial R_y}{\partial y}+\frac{\partial R_z}{\partial z}\right)+Q(x,y,z,t)=\rho C\frac{\partial T(x,y,z,t)}{\partial t} \tag{1}$$

where R_x, R_y and R_z are the rates of heat flow per unit area, $T(x,y,z)$ is the current temperature, $Q(x,y,z)$ is the rate of internal heat generation, ρ is the density, C is the specific heat and t is the time. The model can then be completed by introducing the Fourier heat flow as:

$$R_x=-k_x\frac{\partial T}{\partial x} \tag{2a}$$

$$R_y=-k_y\frac{\partial T}{\partial y} \tag{2b}$$

$$R_z=-k_z\frac{\partial T}{\partial z} \tag{2c}$$

where k_x, k_y and k_z are the thermal conductivities in the x, y and z directions, respectively. Generally, the material parameters k_x, k_y, k_z, ρ and C are temperature dependent. Inserting Eqs. (2a) and (2b) into Eq. (1) yields:

$$\frac{\partial}{\partial x}\left(k_x\frac{\partial T}{\partial x}\right)+\frac{\partial}{\partial y}\left(k_y\frac{\partial T}{\partial y}\right)+\frac{\partial}{\partial z}\left(k_z\frac{\partial T}{\partial z}\right)+Q=\rho C\frac{\partial T}{\partial t} \tag{3}$$

Eq. (3) is the governing differential equation of the thermal part of the problem. The general solution is obtained by applying the following initial and boundary conditions:

$$T(x,y,z,0)=T_0(x,y,z) \tag{4}$$

$$\left(k_x\frac{\partial T}{\partial x}N_x+k_y\frac{\partial T}{\partial y}N_y+k_z\frac{\partial T}{\partial z}N_z\right)+q_s+h_c(T-T_\infty)+h_r(T-T_r)=0 \tag{5}$$

where N_x, N_y and N_z are the direction cosines of the outward drawn normal to the boundary, h_c is the convection heat transfer coefficient, h_r is the radiation heat transfer coefficient, q_s is the boundary heat flux, T_∞ is the surrounding temperature and T_r is the temperature of the radiation heat source. The radiation heat transfer coefficient is expressed as:

$$h_r=\sigma\varepsilon F\left(T^2+T_r^2\right)(T+T_r) \tag{6}$$

where σ is the Stefan–Boltzmann constant, ε is the effective emissivity and F is configuration factor.

Solving Eq. (3) by considering the boundary conditions expressed in Eqs. (4) and (5) gives the temperature distribution in the body. This temperature field will then be applied in the mechanical model to calculate the welding residual stresses and strains (distortions).

In the dissimilar weld joints compared to the similar ones, the physical and mechanical properties vary in different locations of the weld joint (base material and weldment). This makes the governing equations more complicated to be solved compared to the similar joints.

2.2. Mechanical analysis

The equilibrium and constitutive equations used here to conduct elastic–plastic mechanical analysis are described bellow [11].

- Equations of equilibrium:

$$\sigma_{ij,j}+\rho b_i=0 \tag{7}$$

here, σ_{ij} is the stress tensor and b_i is the body force. It is assumed that the stress tensor is symmetrical, i.e. $\sigma_{ij}=\sigma_{ji}$.

- Elastic–plastic constitutive equations:

The thermal elastic–plastic material model, based on the von Mises yield criterion and the isotropic strain hardening rule, is considered. Stress–strain relations are described as:

$$[\mathrm{d}\sigma]=\left[D^{ep}\right][\mathrm{d}\varepsilon]-\left[C^{th}\right]\mathrm{d}T \tag{8a}$$

$$\left[D^{ep}\right]=\left[D^{e}\right]+\left[D^{p}\right] \tag{8b}$$

where $[D^e]$ is the elastic stiffness matrix, $[D^p]$ is the plastic stiffness matrix, $[C^{th}]$ is the thermal stiffness matrix, $\mathrm{d}\sigma$ is the stress increment, $\mathrm{d}\varepsilon$ is the strain increment and $\mathrm{d}T$ is the temperature increment.

Since thermal elastic–plastic analysis is a non-linear problem, the incremental calculation technique is employed here in solving the problem. The incremental stress can be obtained by using the full Newton–Raphson method [2].

3. Experimental investigation

Measurements were conducted to collect data on residual stresses on the outside surface of dissimilar butt-welded joints. The experimental data were used to verify the finite element modelling.

Because of the limitation of the number of test points, the experimental results presented by Mochizuki [5] were also used here.

3.1. Specimen preparation

Two dissimilar pipes, with nominal diameter of 200 mm were prepared with V-groove edges. The materials used here are A106-B carbon steel and A240-TP304 stainless steel. Their chemical compositions are illustrated in Table 1.

Welds were carried out in three passes and welding parameters were controlled cautiously. The parameters used in finite element welding simulation are given in Table 2.

3.2. Measurement of the residual stresses

The hole-drilling method is a standard technique for measuring residual stresses described in detail in ASTM E837 [12]. The stress measurements were made in three points at outer surface of the pipes. These points are located on the weld centre line (point A), 40 mm from the weld centre line in the stainless steel side (point B) and 35 mm in the carbon steel side (point C), as shown in Fig. 1. Strain gages of type FRS-2-1 were mounted on the pipe at selected points to measure the released strains after drilling a hole in the centre point of the gages. The hole was made by using a very high speed drill of RS-200 type. After measuring the released strains by using an indicator of type P-3500, the stresses in the axial and hoop directions are calculated according to the following equations:

$$\sigma_{\max} = \frac{\varepsilon_1+\varepsilon_2}{4A} - \frac{1}{4B}\sqrt{(\varepsilon_3-\varepsilon_1)^2+(\varepsilon_3+\varepsilon_1-2\varepsilon_2)^2} \quad (9)$$

$$\sigma_{\min} = \frac{\varepsilon_1+\varepsilon_2}{4A} + \frac{1}{4B}\sqrt{(\varepsilon_3-\varepsilon_1)^2+(\varepsilon_3+\varepsilon_1-2\varepsilon_2)^2} \quad (10)$$

where ε_1, ε_2, ε_3 are the released strains measured by strain gages. A and B are coefficients related to mechanical properties of the base metal and the hole diameter [12]. Measuring the residual stresses by hole-drilling method is shown in Fig. 2.

4. Finite element calculations

4.1. Welding simulation

The temperature fields and the evolution of the residual stresses are investigated by using finite element method. In order to accurately capture the temperature fields and the residual stresses in the welded pipe, a 3-D finite element model is developed. The thermo-metallurgical behaviour of the weldment during welding is simulated using uncoupled formulation, because the dimensional changes in welding are negligible and the mechanical work done is insignificant compared to the thermal energy from the welding arc. The heat conduction problem is solved independently from the stress problem to obtain temperature history. However, the formulation considers the contributions of the transient temperature field to the stress analysis through the thermal expansion, as well as temperature-dependent thermo-physical and mechanical properties. The material properties of both base metals (A106 and A240) and also filler metal (E38L) are assumed to be temperature dependent. The thermal and mechanical properties of the base metals in different temperature are illustrated in Fig. 3. All analyses are performed using the finite element analysis software ANSYS [13].

Table 1
Chemical composition of base metals.

	C	Cr	Ni	Mo	Mn	Si	P	S	Cu
A106-B	0.3	0.4	–	–	0.27–0.93	0.1	0.035	0.035	0
A240-TP304	0.08	18–20	8–10.5	0.75	2.0	1.0	0.04	0.03	0.75

Table 2
Welding parameters for each pass.

Pass No.	Welding method	Filler	I (A)	V (V)	Travelling speed (mm/s)	Cooling time after welding (s)
1	GTAW	ER 308L	95±5	9	0.55	4500
2	SMAW	E 308L-16	115±5	27–28	3.4–4.1	1100
3	SMAW	E 308L-16	145±5	25–28	2.7–2.8	∞

The FEM modelling used in this study adopts the technique of element birth and death to simulate the deposit filling during the welding. This technique activates or deactivates elements during the analysis, by multiplying their stiffness using a severe reduction factor. Similarly, mass, damping, specific heat, and other such effects are set to zero for deactivated elements. Fig. 4 shows the 3-D finite element mesh for the welded joint used in this study.

4.2. Thermal analysis

During each weld pass, the temperature distribution was calculated from the thermal model. The bead size of each weld pass was determined mainly according to the heat input. The sequence of the weld passes is shown in Fig. 5.

In the present study, the bead shape was not accurately modelled. In this study, the heat of the welding arc was modelled by a surface heat source with a double ellipsoidal distribution proposed by Goldak et al. [14], and that of the molten metal droplets, was modelled by a volumetric heat source.

Pardo and Weckman [15] predicted the weld pool and reinforcement dimensions of welds using a combined heat source. Their research suggests that it seems reasonable that the heat of the metal droplet is assumed to be 60% of the total heat. In this study, the heat of the welding arc was assumed to be 40% of the total heat, and the heat of the molten metal droplets as 60% of the total heat. In multi-pass welding, new elements were added to the mesh periodically after one weld pass was completed. Meanwhile, the heat transfer boundary conditions were modified after the new elements were added. The thermal boundary conditions include the radiation and convection to the environment from all sides of the welded pipe except the area upon which the heat is applied. Radiation losses are dominating for higher temperatures near and

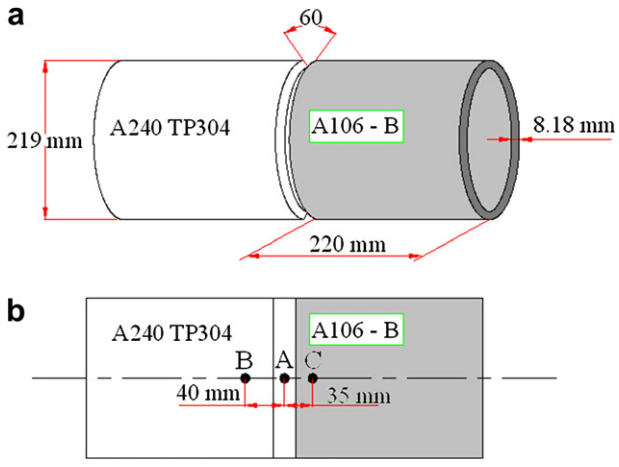

Fig. 1. Dimensional details of specimens (a) test points (b).

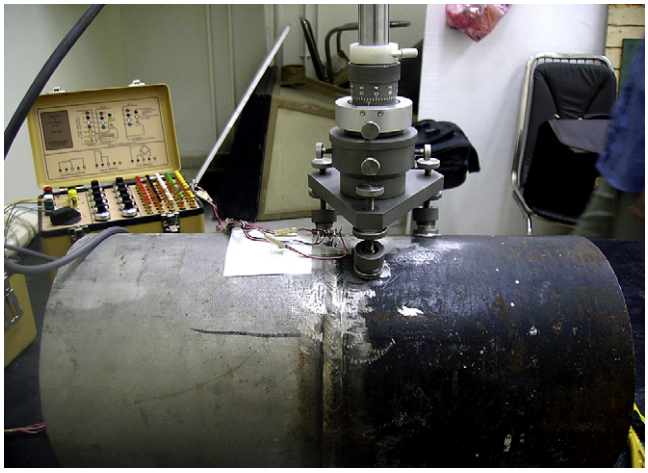

Fig. 2. Hole-drilling measuring of specimen.

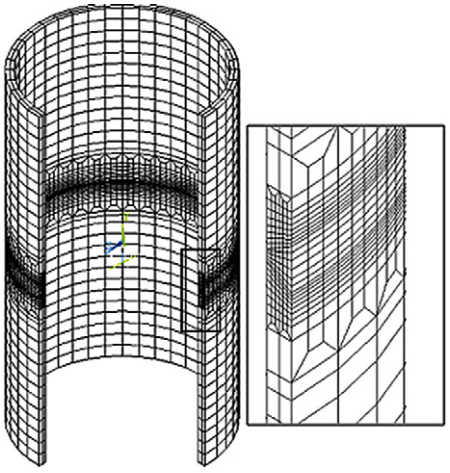

Fig. 4. Finite element mesh used for the butt-weld joint.

in the weld zone, and convection losses for lower temperatures away from the weld zone. A user subroutine was developed to simulate the combined thermal boundary condition. The total temperature-dependent heat transfer coefficient is given by [4].

$$\left\{ \begin{array}{l} \alpha_h = 0.0668T\ (\mathrm{W/m^2}) \quad 0 < T < 500\ ^\circ\mathrm{C} \\ \alpha_h = 0.231T - 82.1\ (\mathrm{W/m^2}) \quad 500 < T\ ^\circ\mathrm{C} \end{array} \right\} \tag{11}$$

where T is the temperature. To simulate heat transfer effects due to fluid flow in the weld pool, the thermal conductivity above the melting temperature was assumed to be doubled [16]. The thermal effects caused by solidification of the weld pool were modelled by considering the latent heat of fusion. In ANSYS, latent heat of phase changes in thermal analysis can be handled using thermal enthalpy method. Here, equivalent specific heat method is adopted to deal with latent heat. Enthalpy can be expressed as:

$$H = \int \rho c(T)\mathrm{d}T \tag{12}$$

The temperature difference of solid phase and liquid phase is ΔT, so the equivalent specific heat is considered as:

$$C^* = H/\rho\Delta T \tag{13}$$

The equivalent specific heat is assumed to be constant in the region between solid phase and liquid phase.

The total net heat input was calculated as:

$$Q = \eta UI/v \tag{14}$$

where η represents the arc efficiency factor, U is arc voltage, I is welding current, and v is the welding speed. The efficiency factor is assumed as 0.6 for the GTAW process, and 0.7 for the SMAW process. The total net heat input of each pass can be calculated based on data given in Table 2. By comparing the temperature versus time at points in different circumferential angle ($\theta = 90^\circ$, 180° and 270°) and same distance from the weld-centre line on the inner surface it can be concluded that the temperature filed is very steady when the welding torch moves around the pipe. From this analysis it was observed that the maximum calculated temperature at the weld pool was around 2200 °C.

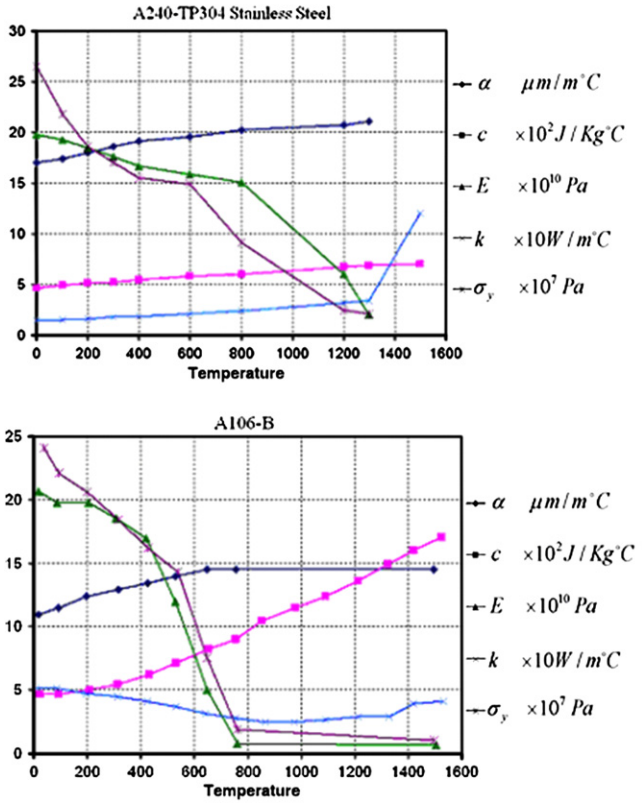

Fig. 3. Temperature-dependent material properties of A240-TP304 stainless steel [18] and A106-B carbon steel [2].

4.3. Mechanical analysis

In the mechanical analysis, the temperature history obtained from the thermal analysis is input into the structural analysis as a thermal loading. Thermal strains and stresses are then calculated at each time increment. In this study volume changes due to

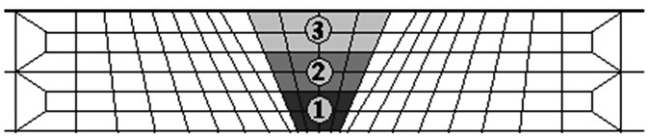

Fig. 5. Sequence of the weld passes.

martensite transformation of the carbon steel side were neglected but the yield stress changes were taken into account. Consideration of phase transformations would result in decreasing in the calculated stresses in the weld and the heat affected zone [17].

During the welding process and neglecting solid-state phase transformation, the total strain rate ($\varepsilon^{\bullet}$) can be written as the sum of the individual components of the strain rate as:

$$\varepsilon^{\bullet} = \varepsilon^{\bullet e} + \varepsilon^{\bullet p} + \varepsilon^{\bullet th} \tag{15}$$

The components in this equation represent strain rate due to elastic, plastic and thermal loading, respectively. The welding residual stresses and strains (distortions) are the accumulated results at the final stage of the calculation, when the whole model is cooled down to the specimen preheat temperature. The materials are assumed to follow the von Mises yield criterion and flow rule. Bilinear kinematic hardening is assumed here.

It can be inferred that the mechanical properties, such as yield strength, alter during cooling. In this study, the yield strength change due to martensite transformation was taken into account by developing a user subroutine. Because of lack of accurate experimental data, we consider yield strength change using a simple method.

The yield strength of the base metal was employed for the model during heating process of the first welding pass. The peak temperature of each integration point in the model was recorded during welding. Depending on the peak temperature that a particular point reached during heating process, decision was made whether the point underwent the austenite–martensite transformation or not. For each point that underwent the phase transformation (just in carbon steel side) the yield strength was replaced by that of the martensite.

In multi-pass welding, because of complicated thermal cycle, some locations will undergo twice or more solid-state phase transformation. For those locations which underwent several times phase transformation, the yield strength of the martensite was used during reheating; because of lack of accurate material data of the low temperature austenite, the yield strength of the base metal was employed during cooling. After the temperature cool down to Ms temperature (Martensite starting temprature) the yield strength of the martensite was applied again. Fig. 6 shows the schematic yield strength change during martensite transformation [18].

To avoid the effects of starting and ending point of welding arc, experimental studies have being done at points with circumferential angle θ equal to 180°.

4.4. FEM verification

Residual stresses in butt-welded pipes develop from the circumferential expansion and contraction during the welding process. Along the weld line, there are high tensile residual stresses near the weld toes, decreasing as the distance from the weld line increases. As the residual stresses in a body are self-balancing, the distribution of the stresses becomes compressive away from the weld zone.

To validate the finite element modelling, FE analysis of a similar pipe weld joint made of JIS STPT410 steel (equivalent to ASTM A106) with the same welding parameters and material properties as used by Mochizuki [5] was conducted. The finite element results were compared with the experimental measurement results presented in [5]. Fig. 7a and b shows the axial stress on the inner and outer surface along the axial direction, respectively, indicating good agreement between the experiment and analysis.

Differences between finite element and experimental results may be because of neglecting the volumetric change in the weld zone caused by austenite to martensite transformation.

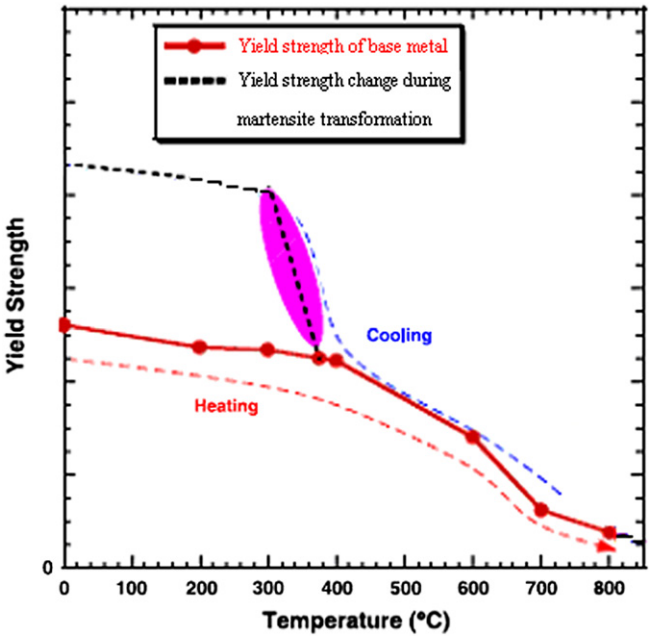

Fig. 6. Yield strength change during martensite transformation.

To verify the result of finite element simulation of the dissimilar pipe weld joint, an FE model with the same geometrical, material and welding parameters with those used for the specimen preparation is generated. Fig. 8 shows the hoop stress on the outside surface along the axial direction. The black spots represent the results of the experimental measurements by the hole-drilling technique. Axial residual stresses obtained from experimental and FE analysis, as shown in Fig. 9. It is observed that the axial residual stresses on the inside and outside surfaces have opposite distribution.

Fig. 10 shows the axial and hoop residual stresses in the axial direction on the inner surface of the dissimilar joint. On the inside surface, the shape of hoop stress distribution is very similar to the axial stress. The peaks of stresses in the dissimilar joint are tend to be in the stainless steel part, and this causes an unbalanced distribution of residual stresses.

To compare the results of the dissimilar joint model with the corresponding solutions for similar pipe joint, an FE model of similar pipe weld joint of 304L stainless steel with same geometries and welding parameters has been prepared.

Fig. 11a and b shows the axial residual stresses in the inner and outer surfaces of this model, respectively. As can be seen, the main difference is that in the similar weld joints, the residual stresses are symmetric in both inner and outer surfaces and the peak stress takes place at the weld centre. But in the dissimilar joint, the peak stresses tend to be in the stainless steel side. It can also be observed that in the outer surface of the dissimilar joint, the maximum tensile stress in the carbon steel part, takes place much closer to the weld centre than that of the similar weld joint.

Axial residual stresses along the weld-centre line through the thickness direction of the similar and dissimilar joints are compared in Fig. 12. As it is shown, the axial residual stresses in both cases change from tensile stresses in the inner surface to compressive stresses in the outer surface.

4.5. Effects of welding heat input

According to Table 3 three cases of different welding heat (h, 0.8h and 0.5h) have been studied here. Distribution of the axial and

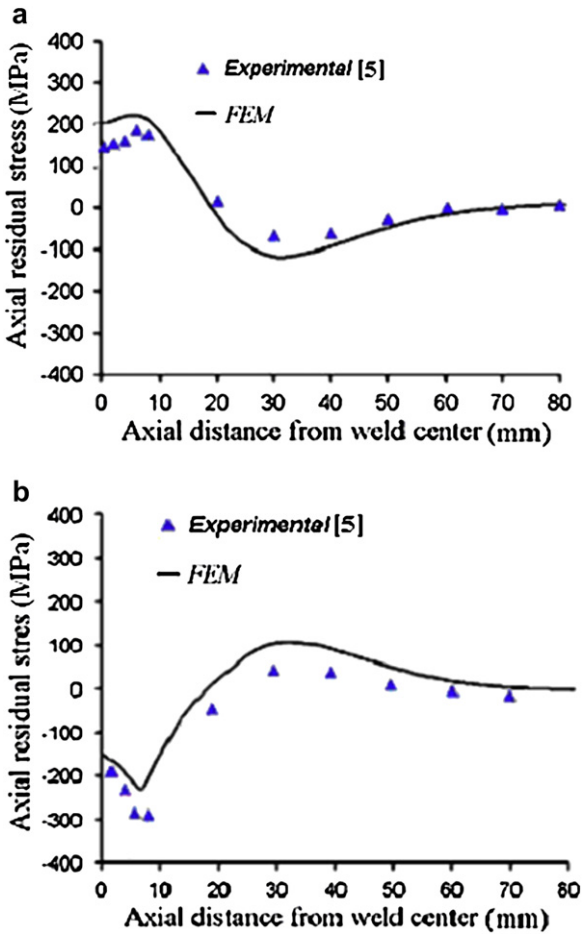

Fig. 7. Axial residual stress in axial direction on the inner surface (a) and outer surface (b) of the pipe, comparison between finite element and experimental data.

hoop residual stresses on the inner surface of dissimilar weld joint, is shown in Fig. 13a and b, respectively.

Fig. 13b shows that the peaks of hoop stresses in these cases do not significantly differ as the heat input is changed. Fig. 13a shows that the peaks of the axial residual stresses decrease from 250 MPa (in heat "h") to 210 MPa (in heat "0.8h") and 160 MPa (in heat "0.5h"). Peaks of the compressive stresses in the stainless steel side

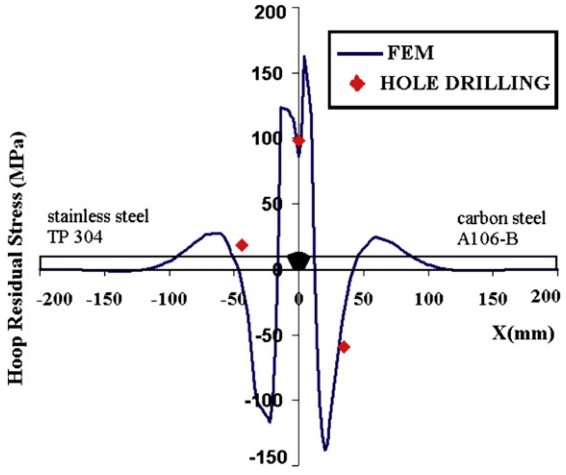

Fig. 8. Hoop residual stress in axial direction on outer surface of dissimilar joint.

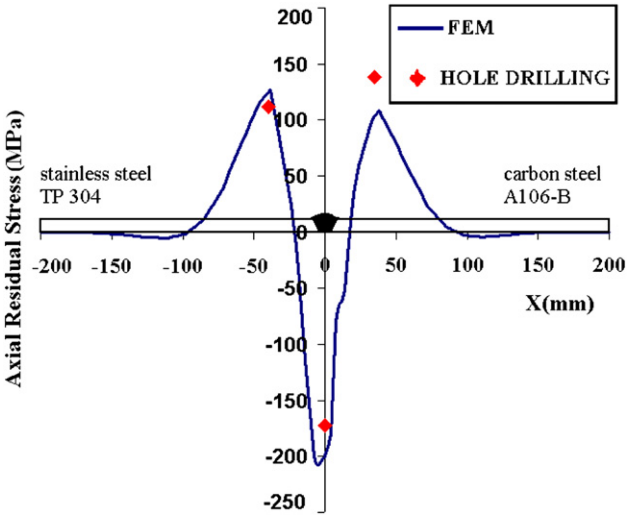

Fig. 9. Axial residual stress in axial direction on outer surface of dissimilar joint.

of joint also decrease as the welding heat input decreases in both axial and circumferential directions. Fig. 13a and b shows that the maximum of the axial compressive stresses in the stainless steel part varies from −155 MPa to −78 MPa and maximum hoop compressive stress varies from −200 MPa to −140 MPa as the heat input is changed from "h" to "0.5h"; But they do not differ in the carbon steel side of the dissimilar joint.

Results of the outer surface also show the same trend. As shown in Fig. 14, the peaks of residual stresses decrease from 130 MPa to 75 MPa as the welding heat increases from "h" to "0.5h" in the stainless steel side. It is observed that they do not differ in the carbon steel side. It is also observed that higher heat input yields to wider distribution of welding residual stresses.

4.6. Discussion

Fig. 13b shows that the peak of residual stress in the weld area, which is in the circumferential direction, is significantly higher than the specified yield stresses of the parent metals in question (265 and 240 MPa). It must be noted from the stress plots that there is significant hydrostatic tension in the fused zone (100–200 MPa)

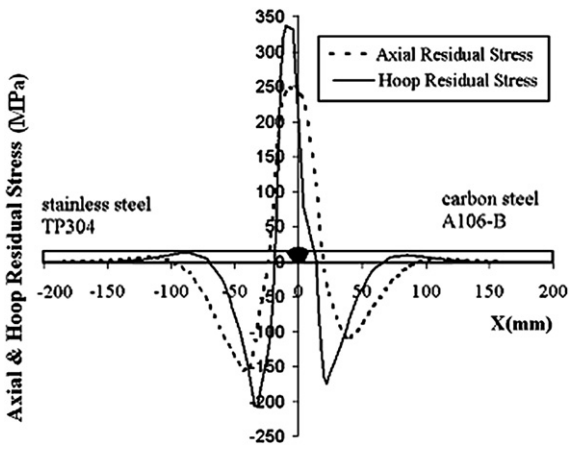

Fig. 10. Axial and hoop residual stresses in axial direction on inner surface of dissimilar joint.

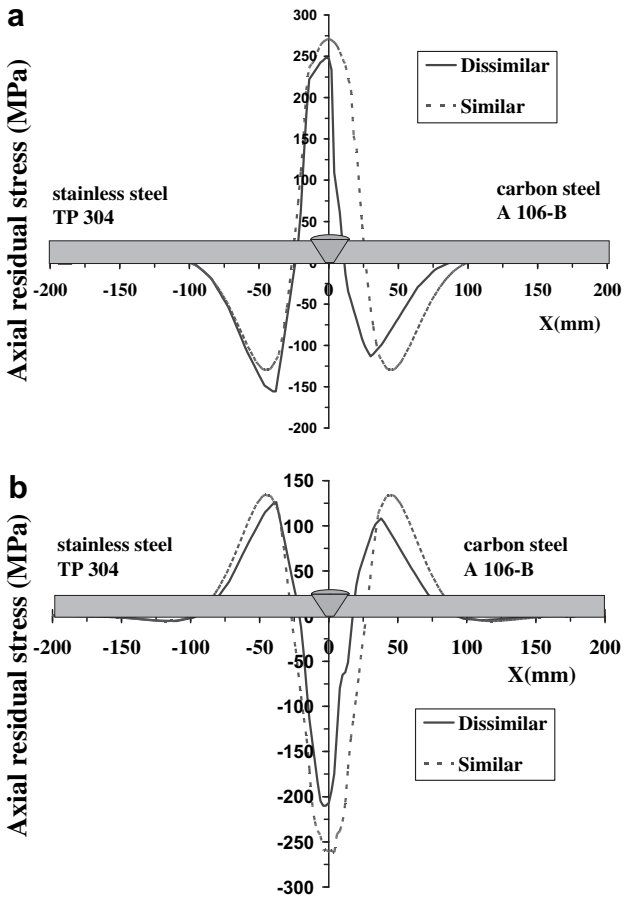

Fig. 11. Axial residual stresses on the inner (a), and the outer (b) surfaces of similar and dissimilar joints.

which means that the maximum principal stresses can be higher than yield.

The main difference between residual stress distributions in similar and dissimilar weld joints is that in similar joints, the distribution of stresses is symmetric. But in dissimilar weld joints of types of this work, the peak stresses (compressive or tensile) tend to be in the stainless steel part. One possible reason may be the higher yield strength of stainless steel TP304 than that of carbon steel A106-B (Fig. 3). The difference between the longitudinal residual stresses in welds of the dissimilar joints increases with increasing yield strength of the materials, as studied in [19].

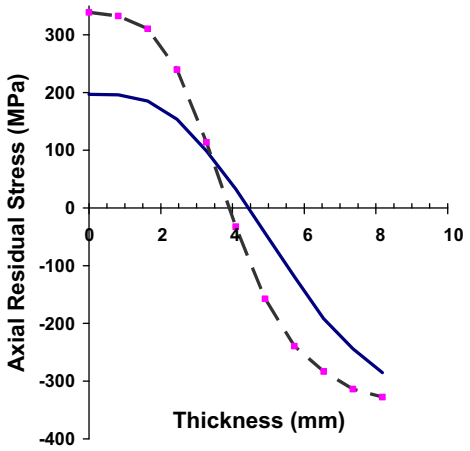

Fig. 12. Axial residual stresses along the weld-centre line through the thickness direction of similar and dissimilar joints.

Table 3
Welding heat input for each pass in three cases.

Case no.	Case name	Heat in pass no. 1 (kJ)	Heat in pass no. 2 (kJ)	Heat in pass no. 3 (kJ)
1	h	900	600	770
2	0.8h	720	480	616
3	0.5h	450	300	360

In the axial direction, maximum compressive residual stress of around three quarters of the maximum value of hoop stress has been observed at the stainless steel, decreasing in the value with the decreasing in the amount of the heat input.

Changing in heat input does not have a significant effect on the peak of stresses in the weld centre line. One possible explanation is that the maximum stress is more affected by yield stress rather than heat input.

It is also observed from Fig. 13 and 14 that decreasing of heat input would decrease the distribution of residual stresses in the stainless steel side more than the carbon steel part. A possible

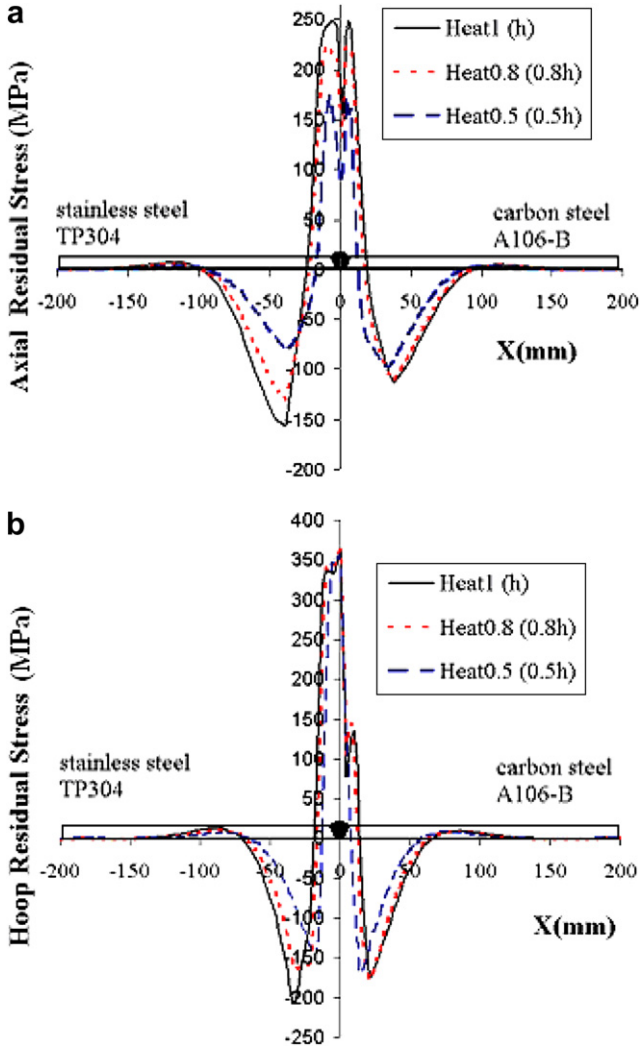

Fig. 13. Axial (a) and hoop (b) residual stresses on the inner surface of the dissimilar joint due to different heat input.

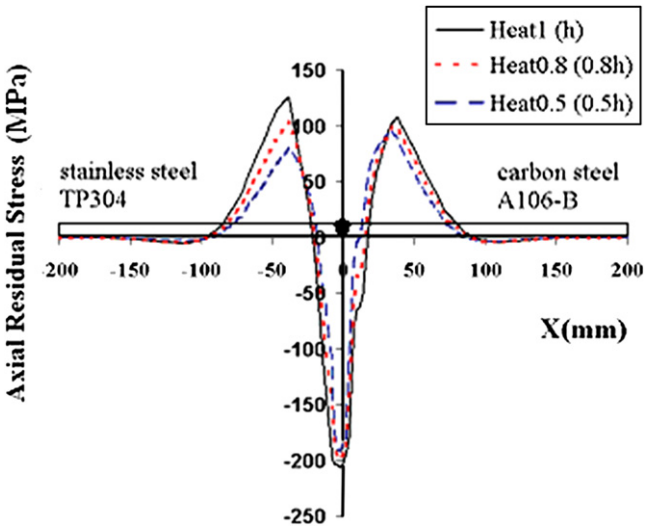

Fig. 14. Axial residual stress on the outer surface of the dissimilar joint due to different heat input.

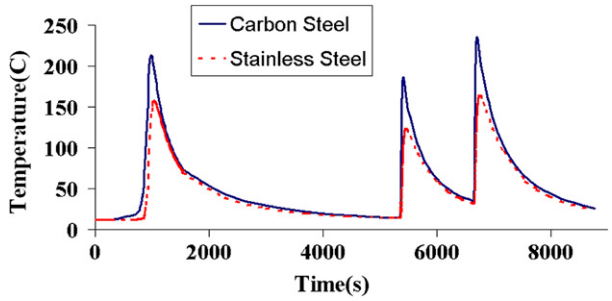

Fig. 15. Time–temperature graph of SS304 and CSA106-B in 40 mm from the weld line.

reason is the effect of decreasing of temperature distribution in the stainless steel. Because the heat distribution coefficient of austenitic stainless steel is much less than that of carbon steel, (about one third) much of the heat input would flow from the carbon steel part, resulting that the temperature of farther points in the stainless steel, is less than that of the carbon steel in the similar points. This fact can be obviously seen in Fig. 15, where the temperature history of two same points in both materials is shown. It is observed that the peak of temperature in carbon steel is higher in all three passes.

5. Conclusions

This research employs the finite element method (FEM) to determine the residual stresses in butt-welds of dissimilar pipe joints. The technique of element birth and death is used to simulate the welding process. By the comparison with the experimental measurements, it has been shown that the proposed computational procedure is an effective method for predicting the welding residual stresses. According to this study, the following conclusions can be made:

1) In the dissimilar weld joint, peak of residual stress in the weld area can be significantly higher than the specified yield stresses of the parent metals.
2) In the dissimilar weld joint of 304 stainless steel to A106 carbon steel, the maximum residual stresses are tend to be in the stainless steel part, and this causes a unbalanced distribution of residual stresses.
3) Peaks of hoop residual stresses do not significantly differ as the heat input changed.
4) Peak of compressive stress in the stainless steel side of joint decreases as the welding heat input decreases in both axial and circumferential direction.
5) Peak of tensile stress in the stainless steel side in the outer surface of this dissimilar pipe weld joint decreases as the welding heat input decreases.
6) In the dissimilar weld joint of stainless steel to carbon steel, decreasing of heat input decreases the distribution of residual stresses in the stainless steel side more than in the carbon steel part.

References

[1] Josepha A, Raib Sanjai K, Jayakumara T, Muruganc N. Evaluation of residual stresses in dissimilar weld joints. International Journal of Pressure Vessels and Piping 2005;82:700–5.
[2] Peng-Hsiang C, Tso-Liang T. Numerical and experimental investigations on the residual stresses of the butt-welded joints. Computational Materials Science 2004;29:511–22.
[3] Paradowska A, Price J, Ibrahim R, Finlayson T. The effect of heat input on residual stress distribution of steel welds measured by neutron diffraction. Journal of Achievements in Materials and Manufacturing Engineering 2006;17:385–8.
[4] Brickstad B, Josefson B. A parametric study of residual stresses in multi-pass butt-welded stainless steel pipes. International Journal of Pressure Vessels and Piping 1998;75:11–25.
[5] Mochizuki M, Hayashi M, Hattori T. Numerical analysis of welding residual stress and its verification using neutron diffraction measurement. Journal of Engineering Materials and Technology 2000:122.
[6] Mohr W. Internal surface residual stresses in girth butt-welded steel pipes. In: ASME, vol. 327; 1996. p. 37–45.
[7] Michaleris P. Residual stress distributions for multi-pass welds in pressure vessels and piping components. In: ASME, vol. 327; 1996. p. 17–27.
[8] Elena S, Mihaela I. FEM application on dissimilar metals welding. Welding Equipment and Technology 2005 ISSN: 1221-4639.
[9] Elena S, Emil C. Effects of welding process on dissimilar metals joints. Welding Equipment and Technology 2001 ISSN: 1221-4639.
[10] Dimitrios E, Anastasius G. Residual stress prediction in dissimilar metal weld pipe joints using the finite element method. Material Science 2005;490–491: 53–61.
[11] Wen-Cheng T. Effect of welding sequences on residual stresses. Computers and Structures 2003;81:273–86.
[12] ASTM E837. Standard test method for determining residual stress by the hole drilling strain gage method. 1995; 3(1).
[13] ANSYS. User's manual. V10. Swanson Analysis System Inc; 2004.
[14] Goldak K, Chakaravarti A, Bibby M. A new finite element model for welding heat sources. Metallurgical Transactions 1984;15B:299–305.
[15] Pardo E, Weckman D. Prediction of weld pool and reinforcement dimensions of GMA welds using a finite element model. Metallurgical Transactions 1989;20B:937–47.
[16] Fenggui L. Modeling and finite element analysis on GTAW arc and weld pool. Computational Materials Science 2004;29:371–8.
[17] Vakarkhan V, Valopot A, Nopa V. Effect of phase transformations on residual stresses in laser welding 09G2 steel. Welding International 2003;17(8):645–9.
[18] Deng D, Murakawa H. Prediction of welding residual stress in multi-pass butt-welded modified 9Cr–1Mo steel pipe considering phase transformation effects. Computational Materials Science 2005.
[19] Chin H, Kyong C. Numerical analysis of residual stresses in welds of similar or dissimilar steel weldments under superimposed tensile loads. Computational Materials Science 2007.